Effect of degree of localization and confinement dimensionality of excitons on their recombination process in CdSe/ZnSe/ZnS$_x$Se$_{1-x}$ single quantum well structures

Shigeo Yamaguchi,* Hitoshi Kurusu, Yoichi Kawakami, Shizuo Fujita, and Shigeo Fujita

Department of Electronic Science and Engineering, Kyoto University, Kyoto 606-01, Japan

(Received 3 March 1999; revised manuscript received 15 October 1999)

We have studied the recombination dynamics of localized excitons in CdSe/ZnSe/ZnS$_x$Se$_{1-x}$ single quantum well structures (SQWS) with the CdSe well layer of 1, 2, and 3 monolayers (MLs). A time-resolved photoluminescence (TRPL) measurement and a nonlinear photoluminescence (NLPL) measurement were used. A time-integrated photoluminescence (TIPL) measurement at 20 K showed that the photoluminescence (PL) from the CdSe layers was observed in the range from the blue spectral region to the green one with increasing CdSe layer width, and that the PL linewidths were about 20–50 meV with an increase in the CdSe layer width. This is resultant from the quantum energy shift and the interfacial roughness between the CdSe and ZnSe layers, respectively. The TRPL measurement showed that excitons were localized at the tail states caused by the interfacial fluctuation. Decay times were measured and found to increase with increasing monitored photon energy, and their values increased with increasing CdSe layer width. It was found that the degree of localization of excitons was larger and the radiative lifetimes of excitons were longer with an increase in the CdSe layer width, indicating that the energy depth in the tail states was smaller and the oscillator strength of excitons was larger for the SQW with a thinner well layer. A NLPL measurement was performed for the 1 and 2 ML SQWS, which revealed that the many-body effect involving localized excitons occurred in the two samples, and that such an effect could result from the localized biexcitons for the 1 ML SQW and from the localized exciton-exciton inelastic scattering for the 2 ML SQW. The difference in the optical properties observed in the two samples is probably due to the difference in the inhomogeneity of the potentials felt by excitons. In order to study the effect of such inhomogeneity on the optical properties of excitons, we investigated the temperature dependence of the TRPL measurement for the three CdSe SQW samples, by which the radiative and the nonradiative lifetimes of localized excitons in the three SQW samples were obtained. These systematic measurements have enabled us to clarify the relationship of localized excitons to both the localization effect and the quantum confinement one. It has been deduced from these results that for a 1 ML SQW, the quantum size effect of excitons is enhanced and the biexcitonic emission is observed, and for 2 and 3 ML SQWS, the degree of localization of excitons becomes larger compared with that for the 1 ML SQW and it prevents excitons from encountering the nonradiative recombination centers.

I. INTRODUCTION

The exciton in II-VI semiconductors has a larger binding energy and smaller Bohr radius compared to those in III-V semiconductors. Accordingly, it is expected that even under high excitation, the Coulomb interaction between electrons and holes is not screened and excitons can remain stable. In fact, various emissions originating from an excitonic many-body interaction have been observed at low temperatures. For example, it has been reported that excitonic molecules (biexcitons)[1] or exciton-exciton inelastic scattering[1] contributes to the formation of optical gain,[2,3] and that for the laser mechanism, excitons that are localized in the tail states due to alloy broadening produce optical gain.[4] This type of localization effect has long been under investigation,[5–10] in particular with much attention paid to bulk crystals such as CdSSe.[11–18] Unlike alloys such as CdSSe, in a ZnCdSe/ZnSSe quantum well (QW) structure, the excitonic localization effect is induced by the interface roughness as well as by the alloy broadening. Understanding and elucidation of the emission mechanism is essential for the optimization of a device structure.

The main factors causing the localization of excitons in QW structures are the interface fluctuation and the alloy composition fluctuation, both of which are inherent in QW structures with any alloy. In addition to such localization effects, for strained QW structures, dislocation and stacking faults induced by the relaxation of strain cause excitons to be localized. In order to restrain the extrinsic localization of excitons due to the poor quality of samples, the QW structures in this study were grown on ZnSSe, which is lattice matched to GaAs substrate, and the thickness of the well was set below the critical thickness.

The CdSe/ZnSe/ZnSSe QW structures assessed here are characterized by the disordered interface that originates from the large strain between CdSe and ZnSe layers. Accordingly, the degree of localization of excitons is expected to be larger than that of the alloy broadening. The degree of localization can be altered only by changing the thickness of the CdSe layer. This enables one to focus on the origin of localization due to the interfacial structure. The CdSe/ZnSe/ZnSSe QW structure is a suitable material for the investigation of strongly localized exciton behavior.[19–21]

Furthermore, localized excitons exhibit the following features. Free excitons should preserve momentum before and after radiative recombination and as a result, an emission process via scattering with optical phonons can take place

even under a high excitation condition. This leads to the nondirect excitonic transition, resulting in a low efficiency of emission. In the localized exciton system, however, momentum conservation is lifted off because of the disordered potentials. This can enhance the possibility of direct transition of excitons. Because excitons become localized in energy and momentum spaces in the disordered potentials, they are restrained from encountering nonradiative centers and thus the enhancement of emission efficiency is expected. In addition, localized states due to the disordered potentials form tail states, where the density of states is small and therefore the population inversion of carriers can easily occur.[4] The localization effect can cause the excitons to possess larger binding energy than free excitons.[22] Indeed, we have recently found experimental evidence that localized biexcitons are the origin of surface emission and edge emission.[21]

II. EXPERIMENTAL PROCEDURE

Time-resolved photoluminescence (TRPL) measurements were carried out using a frequency-doubled beam of a Al_2O_3:Ti laser pumped by a cw Ar^+ laser, and a photon counting method with a synchroscan streak camera in conjunction with a 25-cm single-grating monochromator. The wavelength (WL), the pulse width (PW) and the repetition rate (RR) of the excitation beam were 390 nm, 1.7 ps, and 82 MHz, respectively. The incident excitation energy density was tuned using a variable neutral density filter. The time resolution of the detection system was about 20 ps. Accordingly, the exponential decay time could be estimated within an accuracy of 5 ps by the deconvolution technique.

In order to investigate high excitation effects, nonlinear photoluminescence (PL) spectroscopy was performed by the population mixing technique, in which two excitation beams are modulated at different frequencies ($\Omega = 831$ Hz, $\Omega = 1000$ Hz) by a chopper and focused at the same spot on a sample. A nonlinear PL component was obtained by detecting the sum-frequency element ($\Omega_1 + \Omega_2 = 1831$ Hz) of the total PL signal using a lock-in technique.

In this study, the second harmonic light of the amplified laser output (WL, 400 nm; PW, 200 fs; RR, 250 kHz) was used as an excitation source, and the delay between the excitation pulse pairs was set to be zero. All optical measurements were performed at 20 K using a cryostat.

CdSe/ZnSe/ZnSSe separate confinement single quantum well (SC-SQW) structures studied here were grown by molecular beam epitaxy (MBE) on a Zn-doped p-type GaAs substrate oriented to (100). The growth of the SC-SQW structures was performed as follows. First, a GaAs buffer layer was deposited, followed by a 30-nm-thick ZnSe buffer layer and subsequently, a 0.85-μm-thick $ZnS_{0.07}Se_{0.93}$ cladding layer. The active region, a CdSe SQW sandwiched between ZnSe waveguide layers (each of 50 nm thickness) was grown. Finally, a 0.15-μm-thick $ZnS_{0.07}Se_{0.93}$ capped layer was grown. The mean thickness of the well was set to be 1 ML, 2 ML, or 3 ML. The value was estimated according to the growth rate and PL energy of the CdSe layer. This estimation was in agreement with the previous results for the growth of CdSe on ZnSe,[23] where the CdSe layer thickness was estimated by reflection high-energy electron diffraction
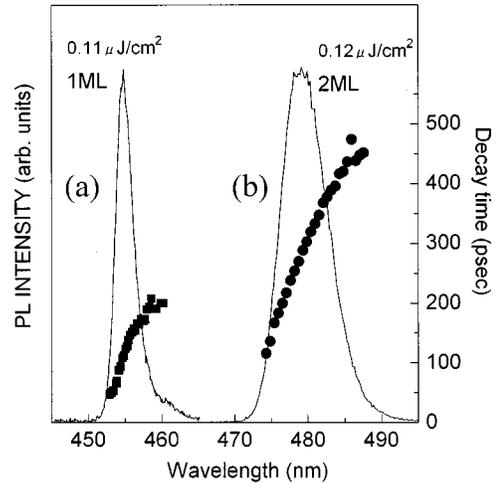

FIG. 1. (a) Time-integrated luminescence spectrum together with decay times for 1 ML SQW under the excitation intensity of 0.11 μJ/cm^2. (b) Time-integrated luminescence spectrum together with decay times for 2 ML SQW under the excitation intensity of 0.12 μJ/cm^2.

(RHEED) oscillation and cross-sectional transmission electron microscopy (TEM).

In Sec. III (III A and III B), excitonic optical properties under a high excitation condition at low temperature are dealt with using 1 and 2 ML SQW samples. Then, in Secs. III C and III D, the temperature dependence of the exciton recombination process under a low excitation condition is dealt with using 1, 2, and 3 ML SQW samples.

III. RESULTS AND DISCUSSION

A. Recombination process under low excitation condition— localization of excitons

Figures 1(a) and 1(b) show time-integrated luminescence (TIL) from the CdSe well layer together with decay times for 1 and 2 ML SQWS under the excitation intensity of 0.11 and 0.12 μJ/cm^2, respectively, which are the lowest excitation intensities for the two samples. The spectral broadening, the full-width at half maximum (FWHM) of the TIL spectra, is about 20 and 40 meV for the 1 and 2 ML SQWS, respectively. The difference in the two values results only from the difference between the microscopic interfacial structure. The CdSe/ZnSe QW system can be characterized by the change of its growth mode from two- to three-dimensions at the stage that the thickness of CdSe is about several MLs; the change of the growth mode is caused by the large lattice mismatch between CdSe and ZnSe layers, and introduces the fluctuation of the interface between CdSe and ZnSe layers. With increasing the CdSe layer width, the interface roughness becomes higher and provides more fluctuated potentials, and accordingly, excitons become localized in the potential minima.[20,21] The difference in the degree of localization of excitons is reflected in the spectral broadening.

These behaviors can be understood in terms of the effect of exciton localization, where the decay of excitons is not only due to radiative recombination but also due to transfer processes to the low-energy tail with the assistance of acoustic phonons.[24,25]

TABLE I. Table of characteristic values for 1 and 2 ML SQWS determined by fitting Eq. (2).

Sample	E_0 (meV)	τ_r (ps)	E_{me} (eV)
1 ML	8.5	209	2.7267
2 ML	16.3	454	2.5914

Those decay curves are well fitted by a single or double exponential curve as in the following expression

$$I(t) = A_f \exp(-t/\tau_f) + A_s \exp(-t/\tau_s), \qquad (1)$$

where τ_f and τ_s are the decay times of the fast and the slow components, and A_f and A_s are constants, respectively. Single exponential approximation is the limiting case for expression (1), with $A_f \gg A_s$.

Using expression (1), decay times for 1 and 2 ML SQWS are plotted (depicted by closed circles) in Figs. 1(a) and 1(b), respectively. The decay times are found to be longer with increasing wavelength; this tendency has been observed in many II-VI alloy semiconductors,[26–33] and has indicated the localization process of excitons. It should be noted that the decay times for the 2 ML SQW are, on the whole, longer than those for the 1 ML SQW. It is most likely that the inhomogeneous broadening of luminescence, namely, the degree of localization, has relevance to the decay times.

In general, the decay time can be related to the degree of localization by the following expression[11]

$$\tau(E)^{-1} = \tau_r^{-1}\{1 + \exp[(E - E_{me})/E_0]\}, \qquad (2)$$

where E_0 is the characteristic energy for the density of states, τ_r is the radiative lifetime, and E_{me} is defined by a definite energy for which the decay time equals the transfer time.

The best fit was obtained for both 1 and 2 ML SQWS as listed in Table I. On the basis of the results listed in Table I, it is found that the energy depth of localized states E_0 is larger for the 2 ML SQW than for the 1 ML SQW and, moreover, τ_r for a 1ML SQW is smaller. Both results indicate the larger oscillator strength of excitons due to the diminution of inhomogeniety in the well layer.

Figures 2 and 3 show the time evolution of the luminescence spectra as a function of time after pulsed excitation (t_d) under the lowest excitation condition for 1 and 2 ML SQWS, respectively. In Fig. 2, the PL peak at $t_d = 0$ ps is located at 454.4 nm (2.728 eV), and then shifts towards a lower photon energy with t_d. This behavior can be understood as a transfer process of excitons to the tail states. The PL spectrum narrows slightly with time from $t_d = 0$ to 40 ps. A shoulder appears and grows at about 458 nm (2.71 eV) after $t_d =$ about 40 ps. The component is overlapped with the main peak (X_1) after $t_d = 400$ ps, and no peak shift is observed afterwards. This indicates that the density of the tail states $[g(E)]$ is not accurately expressed by the form of $\exp[-E/E_0]$ but rather by a form of separately distributed features depending on the interfacial structure. In Fig. 3, the time evolution tendency of the spectra is found to be almost the same as that for the 1 ML SQW. Each spectrum at any t_d is broader compared to that for the 1 ML SQW. This sug-
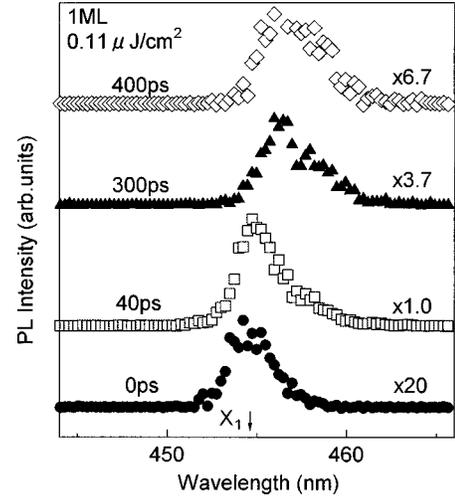

FIG. 2. Time-resolved PL spectra measured as a function of delay time under the excitation intensity of 0.11 μJ/cm^2 for 1 ML SQW.

gests that even at $t_d = 0$, the localization process of excitons has already occurred within the time resolution of the measurement system.

B. Recombination processes under high excitation condition— many-body effect of excitons

As discussed in Sec. III B, the two SQW samples exhibit a difference in the degree of localization of excitons, resulting in a difference in the oscillator strength and in the energy depth of localized excitons. It should be noted that such differences are caused merely by the interface roughness, the inhomogeneity of which may cause excitons to play a significant role in a dense exciton system because the filling of excitons in both phase space and real space may occur simultaneously. On the basis of such an argument, the emission origin may be different between the two samples.

Figures 4 and 5 show the time-integrated luminescence (TIL) spectra from the 1 and 2 ML SQWS, respectively, with
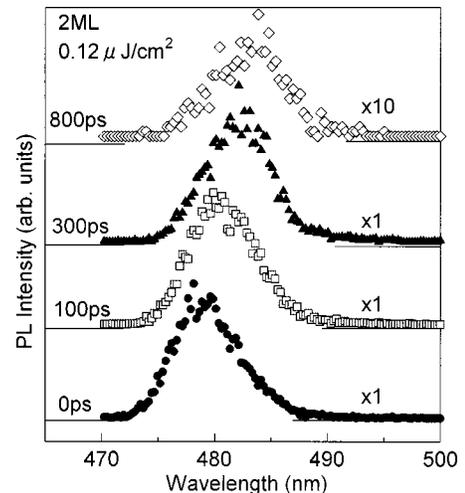

FIG. 3. Time-resolved PL spectra measured as a function of delay time under the excitation intensity of 0.12 μJ/cm^2 for 2 ML SQW.
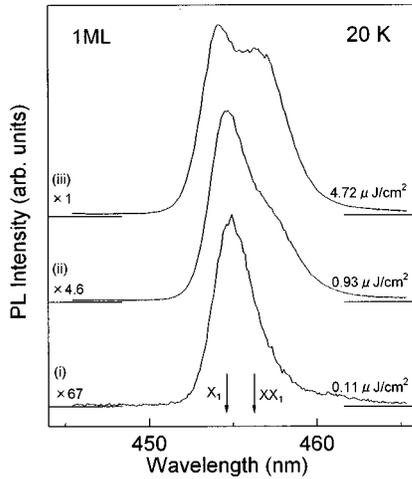
FIG. 4. Time-integrated luminescence spectra for 1 ML SQW with different excitation intensities: (i) 0.11, (ii) 0.93, (iii) 4.72 μJ/cm^2. X_1 and XX_1 denote the main peak and an additional one, respectively.

different excitation intensities: for the 1 ML SQW, (i) 0.11, (ii) 0.93, (iii) 4.72 μJ/cm^2, and for the 2 ML SQW, (i) 0.12, (ii) 2.36, (iii) 5.55 μJ/cm^2.

Some noteworthy features are observed in these figures. Under the lowest excitation intensities, PL spectra exhibited in Figs. 4(i) and 5(i) are dominated by the recombination of localized excitons, with their peaks being situated at 454.61 nm (2.7276 eV) (denoted as X_1) and 479.42 nm (2.5718 eV) for 1 and 2 ML SQWS, respectively. The main peak in Fig. 4(i) gradually shifts to higher photon energies with increasing excitation intensity. This is due to the filling of density of states, which is easily induced for localized excitons lying in the tail state. On the other hand, in Fig. 5, the main peak shifts slightly to a lower energy and then towards higher energies, and further spectral broadening is observed simultaneously.

In Fig. 4, with the raising of the excitation power density to 0.93 μJ/cm^2, a shoulder appears on the lower energy side. With further increasing the excitation intensity, the shoulder
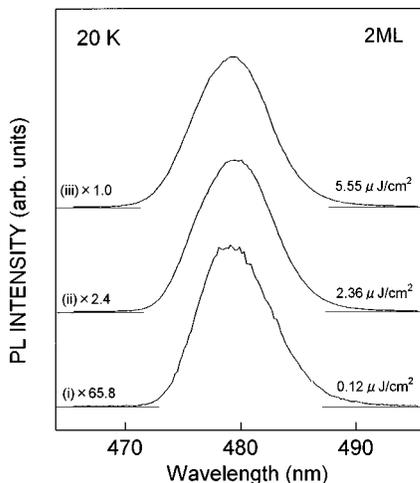

FIG. 5. Time-integrated luminescence spectra for 2 ML SQW with different excitation intensities: (i) 0.12, (ii) 2.36, (iii) 5.55 μJ/cm^2.
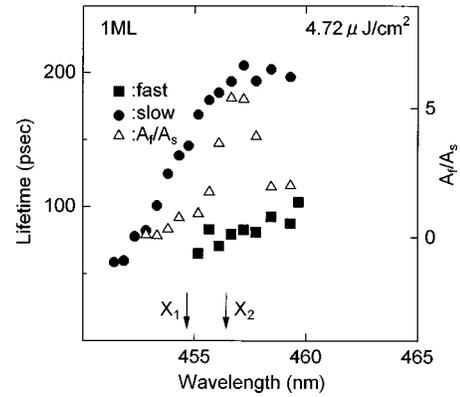

FIG. 6. Fitted values of τ_f, τ_s, and A_f/A_s for 1 ML SQW obtained at the excitation intensity of 4.72 μJ/cm^2.

grows more rapidly than the X_1 line, and an additional peak (denoted as XX_1) emerges at 456.41 nm (2.7168 eV). The energy difference between X_1 and XX_1 is estimated to be about 11 meV.

For 1 ML SQW, the emergence of the additional peak XX_1 and the spectral shift and broadening suggest that the many-body effect involving localized excitons may play a significant role under the high excitation condition. For the 2 ML SQW, although no additial peak is detected in the TIL spectra, the many-body effect of localized excitons probably occurs, judging from the appearance of the spectral shift and broadening.

At this stage, regarding the emission origin for the additional peak XX_1 shown in Fig. 4, a biexcitonic emission process or exciton-exciton inelastic collision is more probable, on the basis of the above discussion and the energy separation of 11 meV. For the 2 ML SQW, the broadness of the TIL spectra makes it difficult to assign the emission origin. However, the peak shift to a lower energy region between the lowest excitation energy density and the second one suggests a contribution of the many-body effect involving localized excitons, although those excitons may be screened by the Coulomb interaction, to separate finally into electron-hole plasma under the highest excitation condition.

On the basis of these results, the many-body effect should be reflected in the decay times, which are smaller under high excitation intensity than those under low excitation intensity. This effect can be observed in Figs. 6 and 7.

The values of decay times are obtained by fitting with expression (1). It should be noted that in Fig. 6 both the slow and the fast decay components increase with decreasing photon energy, indicating that both the X_1 and the XX_1 emission lines are related to localized excitons. The tendency of the slow components in Fig. 6 is almost the same as that of decay times obtained under the excitation intensity of 0.11 μJ/cm^2. The fast components are estimated to be roughly half as small as the slow components, suggesting that the X_1 emission originates from the biexcitonic transition, where a biexciton recombines radiatively leaving a photon and an exciton. This is because the formation rate of biexciton concentration is proportional to the square of exciton concentration after a certain period of pulsed excitation.

On the other hand, in Fig. 7, decay times are found to become smaller in the lower energy region under the high excitation condition, and there is a minimum at about 480
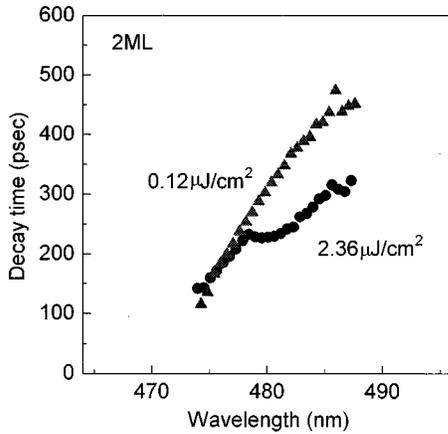
FIG. 7. Fitted values of τ_f for 2 ML SQW obtained at the excitation intensities of (i) 0.12 μJ/cm^2 (closed triangles) and (ii) 2.36 μJ/cm^2 (closed circles).

FIG. 9. Time-resolved PL spectra measured as a function of delay time under the excitation intensity of 2.36 μJ/cm^2 for 2 ML SQW.

nm. The values for the higher energy region remain almost unchanged compared to those under the low excitation condition, implying that the many-body effect occurs principally in the lower energy region. These results strongly suggest that the many-body effect involving localized excitons also occurs in the 2 ML SQW sample.

Figures 8 and 9 show the time evolution of the luminescence spectra as a function of time after pulsed excitation (t_d) under the excitation intensities of 4.72 and 2.36 μJ/cm^2 for 1 and 2 ML SQWS, respectively.

It is found in Fig. 8 that a peak emerges at around X_1 and after 40 ps an additional peak, XX_1, grows rapidly. The X_1 peak gradually shifts towards a lower energy, while the XX_1 peak rapidly diminishes and shows a larger energy shift. It should be noted that the XX_1 peak shows a red shift, strongly indicating the localization process of even biexcitons to the tail states.

The XX_1 line begins to grow at $t_d=$ several tens of ps, reaches the maximum at $t_d=100$ ps, and then decays more rapidly than the X_1 line. The dynamics of localized excitons under the high excitation condition can be described as fol-
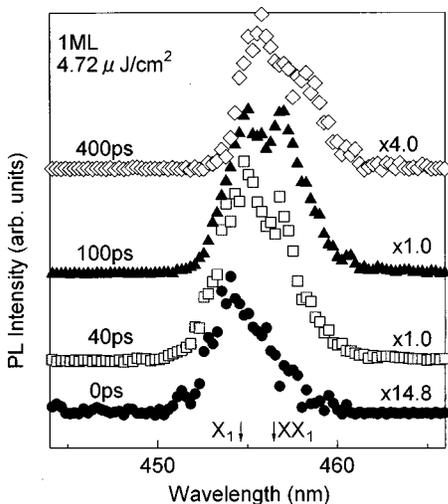
lows. Photogenerated excitons relax to lower energy states and reach the local potential minima. In such a situation, excitons are spatially localized within the well layer due to the break of the momentum preservation, and the many-body effect involving excitons is more easily produced than in the case of flat QWS without the effect of localization.

The energy difference between X_1 and XX_1 is about 11 meV. If the origin of XX_1 is the inelastic collision of excitons, this energy difference should correspond to the binding energy of excitons. However, this cannot be the case here, considering the calculated value of the excitonic binding energy in the sample structure studied here. On the basis of the relationship of decay times between X_1 and XX_1, we can conclude that the radiative recombination of localized biexcitons is the most probable process for XX_1.

For the 2 ML sample, in Fig. 9, the spectrum is observed to be narrower at 300 ps, and additionally, the line shape is seen to be nearly symmetric. Afterwards, however, the spectrum becomes broader again and exhibits a tail in the higher energy region. This transition of the spectral line shape with the delayed time can be explained as follows. Between the delay times of 100 ps and 300 ps, an additional emission with a fast decay component contributes to the sharpening of the line shape, and after several hundred ps, the emission is extinguished.

For the identification of the additonal peak XX_1, for the 1 ML SQW in Fig. 4 and the minimum observed in decay times for the 2 ML SQW in Fig. 7, the nonlinear luminescence measurement was performed.

In general, PL intensity I_{PL} changes with excitation intensity (I_{ex}) according to the following equation. Neglecting the terms higher than the third order, I_{PL} is written as

$$I_{PL}=kI_{ex}^n\approx aI_{ex}+bI_{ex}^2. \tag{3}$$

The signal detected by nonlinear PL spectroscopy is the second term (b) proportional to I_{ex}.

Figures 10 and 11 show the nonlinear PL spectra under three different excitation intensities for 1 and 2 ML SQWS, respectively.

The positive signal indicates the superlinear component, while the negative signal corresponds to the sublinear one, as shown in Fig. 10. For the 1 ML sample, under the low exci-

FIG. 8. Time-resolved PL spectra measured as a function of delay time under the excitation intensity of 4.72 μJ/cm^2 for 1 ML SQW.

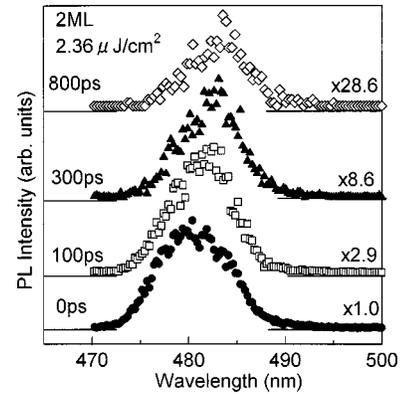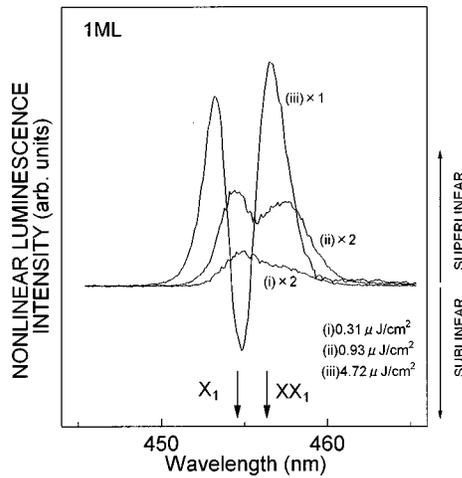FIG. 10. Nonlinear PL spectra under three excitation intensities for 1 ML SQW. (i) 0.31, (ii) 0.93, (iii) 4.72 μJ/cm^2.

tation intensity, the positive signal is observed over the entire spectral range, and the spectral shape is almost the same as the time-integrated linear PL. The origin is probably the saturation of residual nonradiative centers by the photogenerated carriers. Raising the excitation intensity above approximately 0.31 μJ/cm^2, the positive signal at the X_1 line grows more than that at the XX_1 line. Under the excitation intensity of 4.72 μJ/cm^2, the nonlinear signal at the X_1 line changes its sign to negative nonlinearity because of the band-filling effect of localized excitons. However, it should be noted that the positive signal at the XX_1 line continues to grow even at that excitation density, convincingly indicating that the XX_1 line originates from the many-body effect of localized excitons.

For the 2 ML sample SQW, as seen in Fig. 11, a nonlinear signal is obtained for the excitation intensity of more than 0.93 μJ/cm^2. At this excitation intensity, the spectrum indicates twin peaks, both of which correspond to superlinear components. The intensity of the peak located on the low-energy side is higher than that of the peak on the high energy side. At 2.36 μJ/cm^2, the peak located in the low energy region grows more rapidly than the peak in the high energy

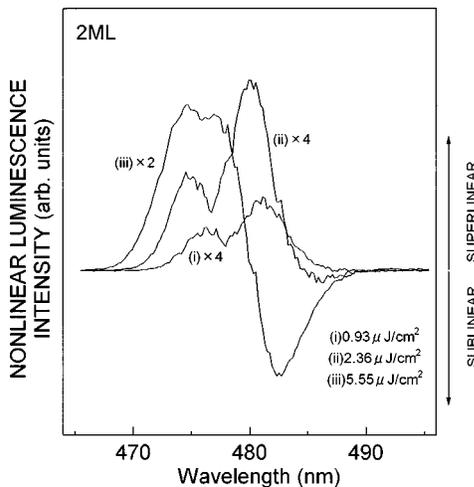region. The energy position of the former peak is found to be situated at a similar position to the minimum as shown in Fig. 7.

Upon further increasing the excitation intensity, the spectrum begins to exhibit a sublinear component on the low energy side, while the superlinear signal is enhanced on the higher-energy side. In addition, the superlinear component in the high energy region exhibits a tail. The change of the sign of the nonlinear signal for the 2 ML SQW represents the reverse tendency in the case for the 1 ML SQW. Namely, in contrast to the 1 ML sample, the nonlinear signal in the lower energy region for the 2 ML SQW saturates earlier than that in the higher energy region, resulting in the contribution of a sublinear component. In Fig. 11, the energy separation between the two peaks observed below 2.36 μJ/cm^2 is estimated to be about 30 meV. Considering that the binding energy of an exciton is calculated to be about 30 meV for the samples assessed in this study, the recombination process under the middle excitation condition for the 2 ML SQW could be attributed to the localized exciton-exciton inelastic scattering. It is clear that under the highest excitation condition, the excitons are screened by the Coulomb interaction to separate them into electron-hole plasma. This is confirmed by the finding that the superlinear component is observed widely in the higher energy region and the saturation process is represented by the sublinear component in the lower energy region.

Therefore, what type of mechanism is the origin for the different radiative recombination processes of excitons for 1 and 2 ML SQWS? We consider this problem as follows. A biexciton is composed of two excitons and, accordingly, has a larger Bohr radius than an exciton. When considering biexcitons and excitons as particles, the biexciton suffers more strongly from the effect of the inhomogeneity of the random potentials. Thus a biexciton is more easily segregated into excitons under strong inhomogeneity.

In the following, we focus on how the difference in the disordered potentials in the CdSe layers influences the optical properties of excitons. We prepared three samples with different well widths of 1, 2, and 3 ML.

Such disorder as described above influences the behavior of excitons. The variation in the depths of the potentials felt by excitons changes the electronic states, and thus the density of the states of excitons is modified. Accordingly, the excitonic absorption and luminescence lines are broadened, through which the behavior of the excitonic localization process can be investigated.

The monochromatic excitation creates localized excitons of a certain energy through no-phonon absorption induced by the random potential. These excitons can either recombine with some probability or transfer towards any exciton state of lower energy. The excitons relax into the localized states where further relaxation and spatial diffusion are possible through tunneling between the localized states. The relaxation rate for this process strongly depends on the density of available final states with lower energies and decreases rapidly with a decrease in energy within the tail states due to the low density of the final states. The decay rate of localized excitons is expressed by the radiative recombination decay rate with relaxation rate to the lower energy states. The de-

FIG. 11. Nonlinear PL spectra under three excitation intensities for 2 ML SQW. (i) 0.93, (ii) 2.36, (iii) 5.55 μJ/cm^2.

TABLE II. Table of characteristic values for 1, 2, and 3 ML SQWS determined by fitting Eq. (2). (Difference between values for 1 and 2 ML SQWs in Table I and Table II is due to the inhomogeneity of the samples.)

Sample	E_0 (meV)	τ_r (ps)	E_{me} (eV)
1 ML	11.2	118	2.7021
2 ML	38.3	364	2.5322
3 ML	56.6	493	2.4470

cay time increases with decreasing photon energy and the TIL peak energy shifts towards lower energies as time passes.[11–17,24–34]

We must bear in mind that such localization is associated with the dimensionality of excitons that is produced by the difference among potentials. Quantum dots (QDs), and quantum wires (QWIs) are considered to be the limiting cases in this respect; therefore, the dimensionality of excitons has been studied.[35–37] In this section, we present experimental results for the enhanced dimensionality due to the random potential. The decay time can be obtained by fitting with expression (1). The best fit has been obtained using the parameters shown in Table II.

C. Time-integrated PL and lifetime

Figures 12(a), 12(b), and 12(c) show a series of time-integrated photoluminescence (TIPL) spectra at 20 K obtained from the CdSe well layer, together with decay times, for 1, 2, and 3 ML CdSe SQWS, respectively, under the excitation intensity of 0.15 μJ/cm^2. The TIPL peak energy is found to shift with the changing of the well width. The TIPL width becomes broader with an increase in the well width.

In Figs. 12(a), 12(b), and 12(c), it is found for all samples that the decay times become longer as photon energy decreases.

On the basis of an argument similar to that in Sec. III B, characteristic values were obtained by fitting with expression (1) and are summarized in Table II. The difference between the 1 ML and 2 ML SQW samples in Tables I and II is due to the slight inhomogeneity of the samples. This is because a
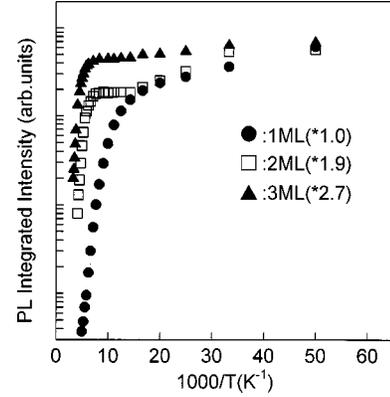
FIG. 13. Temperature dependence of TIPL intensity in an Arrhenius plot for the three SQW samples. The maximum intensities are normalized.

GaAs substrate is not rotated during the growth of epilayers. However, this discrepancy is not considered to be essential in the following discussion.

From Table II, it is found that both E_0 and τ_r are strongly related to the well width, namely, to the degree of randomness of the interfacial structure. τ_r decreases with decreasing CdSe well width, indicating that the oscillator strength of excitons increases. This is confirmed by the finding that the TIPL intensity shown in Fig. 13 is enhanced further as the well width narrows. E_0 increases with increasing well width, indicating the variation of the depth of localized states.

The inhomogeneity can effect the confinement of excitons even for bulk crystals by modifying the wave functions of the excitons through the energy and the momentum spaces.[38,39] It can be considered that as the potential felt by excitons becomes more random, the extent of the wave function of excitons is reduced because the crystal momentum ($>k$) dispersion is widely spread in the dispersion curve, indicating that the diffusion of excitons in real space is prevented and thus they are confined in a certain real region. This phenomenon can be referred to as the dimensionality of the confinement of excitons.[35–37]

D. Temperature dependence of time-integrated luminescence

The localization process of excitons can also be examined in relation to the temperature dependence of TIPL emission. The spatial localization of excitons is further supported by the behavior of the TIPL as a function of the temperature.

Now, it is important to note whether the PL emission is excitonic even at room temperature. The estimated binding energy of excitons in our case (around 30 meV) is slightly larger than the thermal energy at room temperature.[40] However, it should be noted that such excitons can divide into electron-hole pairs with the thermal energy and/or longitudinal optical (LO) phonon energy. Even considering such a situation, the data available for sufficiently high temperatures are convincing as follows.

Figure 14 shows how the emission peak energy shifts and Fig. 15 shows how the FWHM of the TIPL spectra shown in Figs. 12(a), 12(b), and 12(c) varies with temperature, for the three SQW samples. Two features are observed. First, as seen in Fig. 14 for the three samples, within a certain tem-
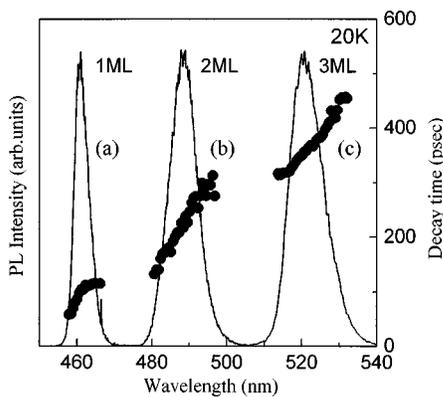

FIG. 12. Time-integrated PL spectrum (solid line) together with decay times (closed circles) obtained at 20 K for (a) 1 ML SQW, (b) for 2 ML SQW, and (c) for 3 ML SQW. The excitation intensity is 0.15 μJ/cm^2 (the same excitation intensity was used for the subsequent experiments below).
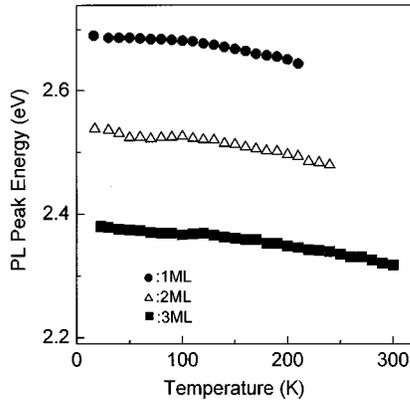
FIG. 14. Temperature dependence of TIPL peak energy for the three SQWS.

perature range, the TIPL peak energy initially moves to a slightly lower energy, followed by an increase in photon energy, after which it again decreases. These anomalous phenomena have been also observed in other materials.[41,42] Second, as shown in Fig. 15, in almost the same temperature range as in Fig. 14, the FWHM first shows an increase, after which it decreases appreciably and then increases again.

This phenomenon is indicative of spatially localized excitons. It can be explained by the behavior of the TIPL peak energy and the FWHM in terms of excitons localized at potential fluctuations in the well layer: as the temperature is raised, the excitons gain greater mobility, increasing the probability that they will become trapped at a lower energy. As the temperature is further increased, the mobile excitons experience more completely the potential fluctuations, producing an increase in the peak emission energy and the FWHM.

The excitons can be regarded as becoming delocalized from the tail states and becoming nearly free at 50 K, 100 K, and 110 K for 1, 2, and 3 ML SQWS, respectively. It should be noted that these characteristic temperatures for the three samples are in good agreement with those in Figs. 13–15. Around each of these characteristic temperatures, a feature is observed; for example, in Fig. 13, for the three samples, the intensity begins to be quenched at the characteristic temperature.

Figure 13 shows an Arrhenius plot of the log of the integrated PL intensity for each well width versus the inverse
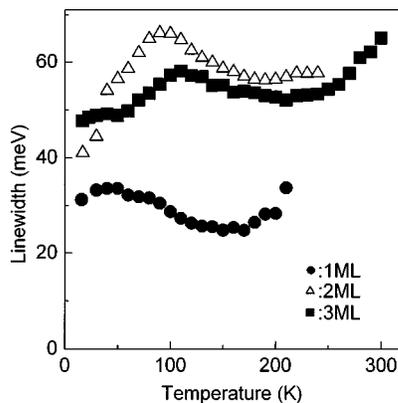

FIG. 15. Temperature dependence of TIPL FWHM for the three SQWS.

temperature. At temperatures at which the thermal quenching starts, the TIPL exhibits a straight-line behavior characterized by an activation energy, 65.5 (1 ML), 187 (2 ML), 203 meV (3 ML). These values may reflect the depth of the trapping of excitons. The three samples exhibit remarkably similar behavior characterized by obeying an Arrhenius dependence. As shown in Fig. 15, the FWHM of TIPL for the 2 ML SQW becomes larger than that for the 3 ML SQW above a temperature of around 50 K. This may result from the difference in the distribution of islands and terraces in the interface between the CdSe and ZnSe layers. This is supported by the results shown in Fig. 13, where, for 2 and 3 ML SQWS, the TIPL intensity is quenched in two steps, and the first activation energy for the 2 ML SQW is larger than that for the 3 ML SQW.

In Fig. 13, at about the characteristic temperature for each sample, the beginning of a decrease in the TIPL intensity is observed. The intensity is reduced by over four orders of magnitude in a small temperature range for the 1 ML SQW, but for 2 and 3 ML SQWS, the ratio of the intensity at a low temperature to that at the highest temperature is found to decrease to 10^{-1}. The intensity at the lowest temperature is larger with decreasing CdSe layer width. However, the temperature at which the TIPL begins to be quenched (almost the same the characteristic temperature in Figs. 14 and 15) is higher with increasing the CdSe layer width. This reflects that at higher temperatures, the nonradiative recombination process plays a larger role for the sample with a thinner well.

The role of the nonradiative recombination process is assessed in the next section.

E. Radiative and nonradiative recombination processes

In Fig. 16(a), the decay times derived from fitting with expression (2) are depicted as a function of temperature for the three SQWS. Measured decay times can be divided into radiative and nonradiative components,[43] and they appear to play different roles in the recombination process for the samples assessed here.

If the PL recombination time, $\tau(T)$ is given by

$$\frac{1}{\tau(T)} = \frac{1}{\tau_r(T)} + \frac{1}{\tau_{nr}(T)}, \qquad (4)$$

where τ is the measured decay time, and $\tau_r(T)$ and $\tau_{nr}(T)$ are the radiative and the nonradiative lifetimes, respectively. Then the temperature dependence of the PL intensity I is given by

$$I = I_0 \frac{\tau(T)}{\tau_r(T)}, \qquad (5)$$

and if separation of $\tau_r(T)$ and $\tau_{nr}(T)$ is possible, the nonradiative recombination process can be assessed quantitatively through the window of decay time.

Because the radiative recombination process is considered to be dominant at the lowest temperature, a purely radiative recombination occurs at $T=20$ K, which yields $I_0 = I(20$ K$)$. Then the following relations are obtained for the radiative and the nonradiative recombination times,
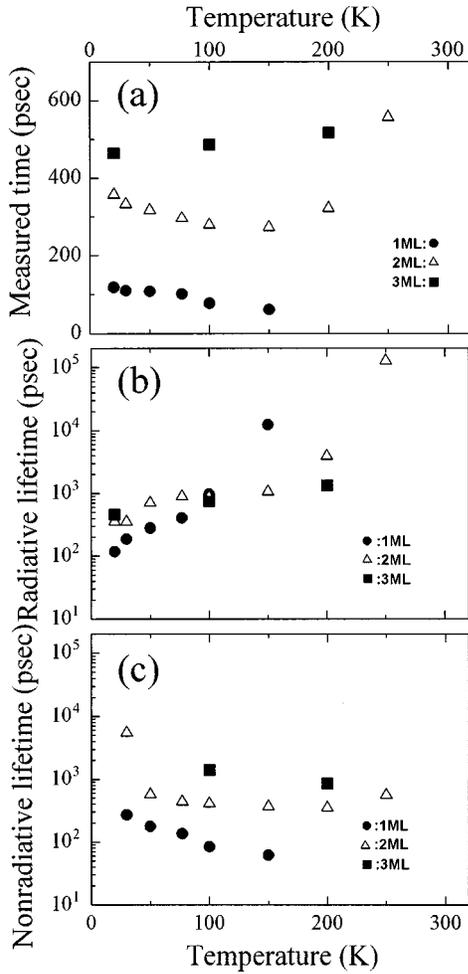
FIG. 16. (a) Measured decay times for the three SQWS. (b) Radiative lifetimes for the three SQWS. (c) Nonradiative lifetimes for the three SQWS.

$$\tau_r(T) = \frac{I(20\ \text{K})}{I(T)}\,\tau(T), \tag{6}$$

$$\tau_{nr}(T) = \frac{I(20\ \text{K})}{I(20\ \text{K}) - I(T)}\,\tau(T). \tag{7}$$

With expressions (6) and (7), the radiative and nonradiative lifetimes are obtained and represented in Figs. 16(b) and 16(c), respectively. In Fig. 16(b), the dependence of τ_r on temperature is clearly distinguished among the three samples. For the 1 ML SQW, in all temperature ranges, τ_r increases with temperature. For 2 and 3 ML SQWS, there are two steps, which reflects the similar tendency seen in Fig. 13.

The dimensionality of the confinement and of the oscillator strength of excitons can be studied in relation to the temperature dependence of τ_r.[35–42] In the lower temperature region, the oscillator strength increases with decreasing CdSe well width, that is, with decreasing inhomogeneous broadening. This implies that the coherency of the wave function of excitons is less disturbed with decreasing inhomogeneity.[38,39] In other words, more excitons with similar k contribute to the enhancement of the oscillator strength. The important point regarding radiative and nonradiative lifetimes is that their inverse values correspond to the prob-

abilities of the recombination passes. Consequently, longer radiative lifetime suggests a difficulty in encountering final states of recombination that are strongly related to the dimensionality. This is due to the limitation of momentum k. In other words, with decreasing the dimensionality, the amount of available k is decreased. On the other hand, smaller nonradiative lifetimes imply the presence of recombination centers without radiation. A more important point is the degree of temperature dependence of the two types of lifetimes. The theory dictates that as the confinement is larger (that is, the dimension is smaller), the temperature dependence of the lifetimes decreases.[35]

It is clear that τ_r is less dependent on temperature with increasing CdSe layer width, that is, with increasing inhomogeneous broadening. For the 1 ML SQW, a stronger dependence is observed in the wide temperature range, indicating that the confinement of excitons becomes weaker and more thermally affected. Below the characteristic temperatures described above, the temperature dependence of τ_r is small. This suggests that the confinement of excitons is further enhanced with increasing inhomogeneity, probably because the coherency of the wave function of excitons is caused to fluctuate by the randomly distributed potentials and thus the amplitude of the wave function is high only in a centered region. Outside this region, the wave function is damped due to its incoherency. Accordingly, excitons are localized at the region in a real space after diffusion within their lifetimes.[20,21,35,38,39]

On the other hand, as seen in Fig. 16(c), τ_{nr} also reflects a situation similar to that for τ_r in terms of the relationship between the dimensionality and the inhomogeneity. τ_{nr} decreases with increasing temperature for the three samples. The inverse of τ_{nr} corresponds to the probability of trapping by nonradiative recombination centers. The values become larger with a decrease in inhomogeneous broadening, and less independent of temperature. These phenomena also support the above description on the basis of the concept of dimensionality. The localized excitons are less mobile and accordingly have less probability of being trapped by the nonradiative centers.

We finally state with clarity for the above mechanism shown in Figs. 16(a)–16(c): with increasing the CdSe layer width, the temperature dependence of both radiative and nonradiative lifetimes decreases, indicating that the confinement dimensionality becomes larger. The difference of this dimensionality in the three SQWS is considered to be due only to the difference in the degree of localization. The localization is produced by the incoherency of the wave function of excitons (or carriers) (it may be useful to recall the Fourier transformation). At least, there is some probability that their existence is in a certain region. Consequently, the larger the degree of localization, the more this region is restricted, and accordingly, excitons (or carriers) become less mobile, leading to the diminution of the probability of meeting nonradiative centers. Figure 16(c) shows that excitons encounter larger nonradiative centers with increasing temperature because they acquire larger thermal energy. This suggests that the samples with smaller well widths have lower confinement dimensionality.

IV. CONCLUSION

We studied the recombination dynamics of localized excitons in CdSe/ZnSe/ZnS$_x$Se$_{1-x}$ single quantum well structures with the CdSe well layer of 1, 2, and 3 monolayers (ML). TRPL measurement and NLPL measurement were used. TIPL measurement showed that decay times increased with increasing the monitored photon energy, and their values increased with increasing the CdSe layer width. It was found that the degree of localization of excitons became larger and the radiative lifetimes of excitons became smaller with an increase in the CdSe layer width, suggesting that the energy depth in the tail states was smaller and the oscillator strength of excitons was larger for the SQW with a thinner well layer. NLPL measurement was performed for the 1 and 2 ML SQWS and showed that the many-body effect including localized excitons occurred in them, and that this effect may result from the localized biexcitons for the 1 ML SQW and from the localized exciton-exciton inelastic scattering for the 2 ML SQW. Using the temperature dependence of the TRPL measurement for the three CdSe SQW samples, the radiative and the nonradiative lifetimes of the localized excitons in them were obtained.

These systematic measurements enabled us to clarify the relationship of localized excitons to both the localization and the quantum confinement effects, and revealed that for the 1 ML SQW, the quantum size effect of excitons was enhanced and the biexcitonic emission was observed, and for 2 and 3 ML SQWS, the degree of localization of excitons became larger compared with that for the 1 ML SQW and it prevented excitons from being trapped by the nonradiative recombination centers.

ACKNOWLEDGMENTS

*Present address: High-Tech Research Center, Meijo University, 1-501 Shiogamaguchi, Tempaku-ku, Nagoya, 468-8502 Japan.

[1] S. Shionoya, H. Saito, E. Hanamura, and O. Akimoto, Solid State Commun. **12**, 223 (1973).

[2] Y. Yamada, K. Yoshimura, S. Fujita, T. Taguchi, F. Sasaki, S. Kobayashi, and T. Tani, Appl. Phys. Lett. **70**, 1429 (1997).

[3] A. Satake, Y. Masumoto, T. Miyajima, T. Asatsuma, F. Nakamura, and M. Ikeda, Phys. Rev. B **57**, R2041 (1998).

[4] J. Ding, H. Jeon, T. Ishihara, M. Hagerott, and A.V. Nurmikko, Phys. Rev. Lett. **69**, 1707 (1992).

[5] J. Puls, V.V. Rossin, F. Kreller, H.-J. Wuensche, St. Renishc, N. Hoffmann, M. Rabe, and F. Hennenberger, J. Cryst. Growth **159**, 784 (1996).

[6] J. Puls, H.-J. Wuensche, and F. Hennenberger, Chem. Phys. **210**, 235 (1996).

[7] G. Kuang, W. Gebhardt, E. Griebl, K. Sube, M. Kastner, M. Woerz, and T. Reisinger, Appl. Phys. Lett. **70**, 2717 (1997).

[8] F. Kreller, J. Puls, and F. Hennenberger, Appl. Phys. Lett. **69**, 2406 (1996).

[9] V. Kozlov, P. Kelkar, A.V. Nurmikko, C.-C. Chu, D.C. Grillo, J. Han, C.G. Hua, and R.L. Gunshor, Phys. Rev. B **53**, 10 837 (1996).

[10] L. Wang, J.H. Simmons, M.H. Jeon, R.M. Park, and C.J. Stanton, J. Electron. Mater. **25**, 177 (1996).

[11] C. Gourdon and P. Lavallard, Phys. Status Solidi B **153**, 641 (1989).

[12] C. Gourdon and P. Lavallard, Phys. Status Solidi B **101**, 767 (1990).

[13] H.-E. Swoboda, F.A. Majumder, C. Klingshirn, S. Shevel, R. Fischer, E.O. Goebel, G. Noll, P. Thomas, S. Pergomorov, and A. Reznitsky, J. Lumin. **38**, 79 (1987).

[14] S. Shevel, R. Fischer, E.O. Goebel, G. Noll, P. Thomas, and C. Klingshirn, J. Lumin. **37**, 45 (1987).

[15] H. Schwab, V.G. Lyssenko, J.M. Hvam, and C. Klingshirn, Phys. Rev. B **44**, 3413 (1991).

[16] J.A. Kash, A. Ron, and E. Cohen, Phys. Rev. B **28**, 6147 (1983).

[17] S. Permogorov, A. Retnitskii, S. Verbin, G.O. Mueller, P. Floegel, and M. Nikiforova, Phys. Status Solidi B **113**, 589 (1982).

[18] H.X. Jiang, L.Q. Zu, and J.Y. Lin, Phys. Rev. B **42**, 7284 (1990).

[19] F. Yang, G.R. Hayes, R.T. Phillips, and K.P. O'Donnell, Phys. Rev. B **53**, R1697 (1996).

[20] S. Yamaguchi, Y. Kawakami, Sz. Fujita, Sg. Fujita, Y. Yamada, T. Mishina, and Y. Masumoto, Phys. Rev. B **54**, 2629 (1996).

[21] S. Yamaguchi, H. Kurusu, Y. Kawakami, Sz. Fujita, and Sg. Fujita, Superlattices Microstruct. **23**, 1189 (1998).

[22] M. Sugawara, Jpn. J. Appl. Phys., Part 1 **35**, 124 (1996).

[23] Sz. Fujita, Y.-H. Wu, Y. Kawakami, and Sg. Fujita, J. Appl. Phys. **72**, 5233 (1992).

[24] E. Cohen and M.D. Sturge, Phys. Rev. B **25**, 3828 (1982).

[25] S. Permogorov and A. Reznitsky, J. Lumin. **52**, 201 (1992).

[26] H. Kalt, J. Collet, S.D. Baranovskii, R. Saleh, P. Thomas, L.S. Dang, and J. Cibert, Phys. Rev. B **45**, 4253 (1992)

[27] Y. Hefetz, D. Lee, A.V. Nurmikko, S. Sirananthan, X. Chu, and J.-P. Faurie, Phys. Rev. B **34**, 4423 (1986).

[28] R.P. Stanley, J.F. Donegan, J. Hegarty, R.D. Feldman, and R.F. Austin, J. Lumin. **52**, 109 (1992).

[29] J.P. Doran, R.P. Stanley, J.F. Donegan, J. Hegarty, R. Fischer, E.O. Goebel, R.D. Feldman, and R.F. Austin, Physica B **185**, 566 (1993).

[30] L.G. Suslina, A.G. Plyuknin, O. Goede, and D. Henning, Phys. Status Solidi B **94**, K185 (1979).

[31] A. Reznitsky, S. Permogorov, S. Verbin, A. Namauv, Ya. Kolostein, V. Noroznikov, and S. Prokv'ev, Solid State Commun. **52**, 13 (1984).

[32] E.I. Rashba and F.T. Pohupr, Fiz. Tekh. Poluprovodn. **8**, 1241 (1974) [Sov. Phys. Semicond. **8**, 808 (1975)].

[33] Y. Kawakami, M. Funato, Sz. Fujita, Sg. Fujita, Y. Yamada, and Y. Masumoto, Phys. Rev. B **50**, 14 655 (1994).

[34] W. Maier and C. Klingshirn, Solid State Commun. **28**, 13 (1978).

[35] H. Gotoh, H. Ando, T. Takagahara, H. Kamada, A.C. Pirson, and J. Temmyo, Jpn. J. Appl. Phys., Part 1 **36**, 4204 (1997).

[36] J. Feldmann, G. Peter, E.O. Goebel, P. Dawson, K. Moore, C. Foxon, and R.J. Elliot, Phys. Rev. Lett. **59**, 2337 (1987).

[37] H. Akiyama, S. Koshiba, T. Someya, K. Wada, H. Noge, Y. Nakamura, T. Inoshita, A. Shimizu, and H. Sakaki, Phys. Rev. Lett. **72**, 924 (1994).

[38] N.F. Mott, Philos. Mag. **13**, 989 (1966).

[39] M.H. Cohen, H. Fritzsche, and S.R. Ovsshinsky, Phys. Rev. Lett. **22**, 1063 (1969).

[40] J. Singh and K. K. Bajaj, J. Appl. Phys. **57**, 5433 (1985).

[41] M. Kondow, S. Minagawa, Y. Inoue, T. Nishino, and Y. Ha-makawa, Appl. Phys. Lett. **54**, 1760 (1989).

[42] R.P. Schneider, Jr., E.D. Jones, J.A. Lott, and R.P. Bryan, J. Appl. Phys. **72**, 5397 (1992).

[43] M. Guriolim, A. Vinattieri, M. Colocci, C. Deparis, J. Massies, G. Neu, A. Bosacchi, and S. Franchi, Phys. Rev. B **44**, 3115 (1991).